HHS Public Access

Author manuscript

Nat Biotechnol. Author manuscript; available in PMC 2015 July 01.

Published in final edited form as:

Nat Biotechnol. 2015 January ; 33(1): 64–72. doi:10.1038/nbt.3071.

Injectable, spontaneously assembling inorganic scaffolds modulate immune cells *in vivo* and increase vaccine efficacy

Jaeyun Kim[1,2,3,5], **Weiwei Aileen Li**[1,2,5], **Youngjin Choi**[3], **Sarah A. Lewin**[2], **Catia S. Verbeke**[1,2], **Glenn Dranoff**[4], and **David J. Mooney**[1,2]

[1]School of Engineering and Applied Sciences, Harvard University, Cambridge, MA, USA.

[2]The Wyss Institute for Biologically Inspired Engineering, Harvard University, Boston, MA, USA.

[3]School of Chemical Engineering, Sungkyunkwan University, Suwon, Korea.

[4]Dana-Farber Cancer Institute and Harvard Medical School, Boston, MA, USA.

Abstract

Materials implanted in the body to program host immune cells are a promising alternative to transplantation of *ex vivo*–manipulated cells to direct an immune response, but required a surgical procedure. Here we demonstrate that high-aspectratio, mesoporous silica rods (MSRs) injected with a needle spontaneously assemble *in vivo* to form macroporous structures that provide a 3D cellular microenvironment for host immune cells. In mice, substantial numbers of DCs are recruited to the pores between the scaffold rods. The recruitment of DCs and their subsequent homing to lymph nodes can be modulated by sustained release of inflammatory signals and adjuvants from the scaffold. Moreover, injection of an MSR-based vaccine formulation enhances systemic T_H1 and T_H2 serum antibody and cytotoxic T cell levels compared to bolus controls. These findings suggest that injectable MSRs may serve as a multifunctional vaccine platform to modulate host immune cell function and provoke adaptive immune responses.

Keywords

porous scaffold; cellular microenvironments; mesoporous silica; immunotherapy; *in vivo* cell recruitment

Although recent clinical successes with immunotherapies demonstrate their potential[1,2], in most cases it remains difficult to generate sufficiently robust immune responses to achieve lasting therapeutic success. Biomaterials may be useful to enhance the effectiveness of

Correspondence should be addressed to D.J.M. (mooneyd@seas.harvard.edu).

[5]These authors contributed equally to this work.

AUTHOR CONTRIBUTIONS

J.K., W.A.L. and D.J.M. conceived and designed the experiments. J.K., W.A.L., Y.C., S.A.L. and C.S.V. performed the experiments. J.K., W.A.L., G.D. and D.J.M. analyzed the data. J.K., A.L. and D.J.M. wrote the manuscript. All authors discussed the results and commented on the manuscript. J.K. and A.L. equally contributed to this work. The principal investigator is D.J.M.

COMPETING FINANTIAL INTERESTS

The authors declare no competing financial interests.

vaccines and other immunotherapies[3–8]. The design and fabrication of porous materials has been intensively investigated to pursue new material properties for a variety of applications including cell/tissue engineering and regenerative medicine[9–11]. Recently, it has been proposed that *in vivo* modulation of host cell populations can be achieved using 3D biomaterials with spatiotemporal control of biochemical and mechanical cues[3,12–14]. However, 3D biomaterials are typically fabricated *in vitro*, requiring surgical placement in the body, and their preformed structures could limit the capability of host cells to organize themselves.

Here we propose an approach in which host immune cells are recruited and modulated *in vivo* by 3D scaffolds that spontaneously assemble from mesoporous silica rods (MSRs) of high aspect ratio (Fig. 1). Owing to their high pore volume and large surface area, mesoporous silica has been intensively investigated for controlled drug release[15–17]. In general, synthetic amorphous silica is known to have good biocompatibility[18,19], supporting its development as a versatile platform for clinical applications. In this study, we describe injectable pore-forming scaffolds based on MSRs, and demonstrate their application to *in vivo* modulation of host immune cells, and potential as a vaccine platform to provoke adaptive immune responses.

RESULTS

Injected MSRs spontaneously form a 3D microenvironment

We first hypothesized that rod-shaped mesoporous silica particles with high aspect ratio could non-specifically assemble, or coalesce to form structures with significant interparticle spaces (pores) upon subcutaneous injection *in vivo*. If interparticle pores generated by particle assembly are bigger than the size of cells, host cells could potentially infiltrate into that space. To test this idea, MSRs with a hexagonal mesoporous structure were synthesized through the silica sol-gel reaction in the presence of a pore-directing agent, Pluronic block copolymer P123[20,21]. The MSRs were, on average, 88 μm in length and 4.5 μm in diameter as measured by SEM (Fig. 2a, left), and had cylindrical mesopores as measured by TEM (Fig. 2a, right). The N_2 adsorption/desorption isotherms exhibited a type IV isotherm with a hysteresis loop[20], demonstrating the mesoporous characteristic of the MSR (Supplementary Fig. 1a) with 10.9 nm pore size (Supplementary Fig. 1b). The BET surface area and the total pore volume were 703 $m^2\ g^{-1}$ and 1.33 $cm^3\ g^{-1}$, respectively. SEM imaging of MSRs on a model substrate demonstrated random particle assembly, with interparticle spaces of tens of micrometers (Fig. 2a). To test if the MSRs could be randomly assembled *in vivo*, MSRs dispersed in PBS were injected via needle into the dorsal flank of mice. A large bump was formed immediately after injection due to the volume of the buffer. The outward diffusion of the dispersion buffer occurred in less than 30 min, and led to the disappearance of the initial bump. At around 4 h, a small nodule began to form. The size of the nodule increased over time (Fig. 2b) and remained apparent for at least two weeks. To examine if the injected MSRs were assembled, MSRs conjugated covalently with rhodamine dye were injected, and the nodule was isolated after 24 h. Fluorescent microscopy revealed a random assembly of MSRs into 3D structures with interparticle spaces (Fig. 2c), as observed with SEM *in vitro* (Fig. 2a).

MSR scaffold is capable of recruiting host cells

Next, the ability of host cells to infiltrate the interparticle pores of injected MSR scaffolds *in vivo* was examined. MSRs were again injected into subcutaneous tissue of mice, and the nodule was retrieved at designated time points. The injection of MSRs did not induce a noticeable wound in the skin of the mice. The histology of nodules retrieved on day 3 demonstrated high cellular infiltration into the interparticle spaces and almost no collagen deposition nor fibroblast infiltration (Fig. 2d). Nodules retrieved at day 7 (Fig. 2e) were analyzed with SEM, confirming they were composed of a high number of cells that completely occupied the structure (Fig. 2f and Supplementary Fig. 2). Removal of the cells, followed by SEM imaging revealed the underlying structure formed by the injected MSRs (Fig. 2g). The isolated cells showed more than 90% viability (Fig. 2h).

As interparticle pores formed through the spontaneous assembly of particles with elongated shapes, we hypothesized that longer MSRs with higher aspect ratio would lead to the formation of larger spaces than particles with lower aspect ratio, thus providing more room for cells to infiltrate. Higher (88 × 4.5 μm in length and diameter) and lower (37 × 3.2 μm in length and diameter, Supplementary Fig. 3) aspect ratio MSRs were synthesized and injected subcutaneously, and the numbers of recruited cells were analyzed on day 7 post injection. As hypothesized, higher aspect ratio MSRs led to 2.5-fold more cells residing in the structures than lower aspect ratio MSRs (Fig. 2i, **left**). Fifty three million cells were recruited to structures formed from the high aspect ratio particles (20 mg). To determine whether the number of recruited cells is overestimated due to background cell counts, we extracted MSRs from mice that had been injected only 20 min earlier. The cell number was 22 times fewer than that found after 24 hours, and 374 times fewer than after 5 days, indicating cells measured in the MSR scaffolds were recruited over time, and not contaminating cells from the surrounding tissue. As an innate immune response is likely induced upon injection of MSRs, the presence of $CD11c^+$ DCs, important professional antigen presenting cells that bridge innate and adaptive immunity, was analyzed. MSR injection and assembly led to the recruitment of 15 million $CD11c^+$ DCs to the high aspect ratio MSRs, which is a 2.5-fold increase as compared to structures from the lower aspect ratio particles (Fig. 2i, **right**). These results indicate that simple, injectable MSRs provide a material platform for infiltration of large numbers of host immune cells. As the macroporous structure is spontaneously generated *in vivo*, this spontaneously assembling scaffold allows one to bypass *ex vivo* synthesis of the scaffold and to minimize geometric and spatial constraints of a preformed scaffold.

To determine the role of mesopores and macropores in recruiting cells, we compared cell recruitment using two control materials based on MSRs. One was pore-filled silica microrods with the same aspect ratio and morphology, but almost no mesoporosity compared to MSRs (Supplementary Fig. 4a–c). The other control was monolith-type (pressed) MSRs maintaining the intrinsic mesopores of MSRs but lacking interparticle macropores (Supplementary Fig. 4d–e). The numbers of host cells recruited at day 3 into the same mass of both pore-filled silica microrods and pressed MSRs were significantly lower than pristine MSRs (Fig. 2j). This result clearly indicates that the interparticle macropores formed by MSR assembly are crucial to recruit a high number of cells. This result also

indicates that a constant mass of MSRs is more effective than non-porous silica rods, likely because a higher number of MSR particles is present at constant mass due to their lower density, resulting in more interparticle macropores.

The biodegradability of biomaterials is an important issue in the body. It is known that mesoporous silica can degrade into silicic acid *in vitro* and *in vivo* over time[22–24]. To indirectly investigate *in vivo* degradation and clearance of the MSR scaffolds in injection site, we measured the size of the subcutaneous nodule over time after injection of blank MSRs (Fig. 2k). The nodule increased in size until day 7, and was reduced to an almost unmeasurable size after 25 days. Fluorescent imaging of sections of the nodule retrieved at day 7 after injection of fluorescent protein-adsorbed labeled MSRs showed the random assembly of MSRs surrounded by the recruited cells (Fig. 2l and Supplementary Movie 1), while the sectioned nodule at day 28 showed very few MSRs (Fig. 2m and Supplementary Movie 2). These results indicate that the injected MSRs were significantly degraded *in vivo* after subcutaneous injection. There was no significant toxicity or inflammation in liver, kidney, or other organs of the mice injected with MSRs. We did not observe any difference in animal behavior after injection compared to naïve animals. Animals appeared to tolerate well the injections, and made no efforts to disturb the injection site, suggesting it did not present significant discomfort or pain.

Sustained release of signaling molecules from MSR-scaffold

The ability of small signaling molecules to be loaded into the pores of the MSRs and released from the particles in a sustained manner was next examined. First, incorporation of a cytokine, granulocyte-macrophage colony-stimulating factor (GM-CSF), a potent stimulator of dendritic-cell recruitment and proliferation[25,26], was examined. The release of GM-CSF, measured with radioactive factor, showed a typical burst of release followed by a sustained release of 66% of the total loaded GM-CSF by day 40 (Supplementary Fig. 5), while the release measured by ELISA shows nearly first-order release with lower level of bioactive GM-CSF released (Fig. 3a). The released GM-CSF resulted in *in vitro* BMDC proliferation, indicating the continuous release of bioactive GM-CSF for at least 35 days. We hypothesized that the recruitment of immature DCs could be enhanced by GM-CSF release, and MSRs (5 mg) loaded with 0, 500, 1000, or 3000 ng of GM-CSF were injected into subcutaneous tissue, and subsequently retrieved to analyze the DC population. $CD11c^+$ $CD11b^+$, a widely accepted marker for conventional DCs was used to determine DC numbers. In addition, the expression levels of a costimulatory surface marker, CD86, and the major histocompatibility complex, MHC II, were used to assess DC activation[27,28]. Dose dependent increases in $CD11c^+$ $CD11b^+$, and $CD11c^+$ MHC II^+ DCs were found in the scaffolds with GM-CSF release (Fig. 3b). The numbers of total cells and DCs were still maintained higher in vaccine scaffolds than in blank scaffold at day 14 (Supplementary Fig. 6).

Next, the ability of MSRs to provide cues to modulate the phenotype of DCs was analyzed. To efficiently mature DCs, danger signals containing conserved molecular patterns present in common infectious agents, termed pathogen associated molecular patterns (PAMPs), are required to bind to pattern recognition receptors such as Toll like receptors (TLRs)[29]. The

unmethylated cytosine-phosphate-guanine oligonucleotide (CpG-ODN) sequence, a potent agonist for TLR9, was used in this study, as previous studies have shown that vaccines containing CpG-ODN can elicit strong CD8 killer T cell mediated immune responses[30]. *In vitro*, a burst of CpG-ODN release was followed by a sustained release at a much lower rate (Fig. 3c). To evaluate whether co-loading of CpG-ODN with GM-CSF could activate DCs *in vivo*, the expression of CD86 and MHC II in DCs retrieved from MSR releasing solely GM-CSF (MSR-GM), and MSR releasing both GM-CSF and CpG-ODN (MSR-GM-CpG) at day 3 post injection was analyzed. MSR-GM-CpG yielded 1.3- and 2.5-fold increases in the number of recruited DCs expressing $CD86^+$ and MHC II^+, as compared to MSR-GM (Fig. 3d and Supplementary Fig. 7). As the level of endotoxin in the MSRs was below the detection limit of the endotoxin assay, the activation of DCs was not derived from undesired contamination of MSRs.

We next verified that MSRs can be loaded with protein antigens, and present them in a sustained manner. *In vitro*, OVA was released relatively quickly, with ~45% released within 5 days (Supplementary Fig. 8). To investigate *in vivo* release of OVA from MSRs, MSRs were loaded with Alexafluor 647-labeled OVA (MSR-OVA*), and the duration of OVA* presence at the vaccine site was compared to the injection of bolus OVA*, using near infrared fluorescent imaging (Fig. 3e). The fluorescence at the site of bolus OVA* injection decreased to 10% of the initial level by day 1 post injection, while the MSR-OVA* condition maintained 60% of the initial OVA* level at this time point. At day 10 post injection, the OVA remaining at the vaccination site was still 10.6-fold higher in MSR-OVA* than in the bolus OVA* condition, suggesting that MSRs are a good candidate for sustained release of antigenic proteins in microenvironments housing antigen presenting cells.

MSR vaccine modulates DCs to exert systemic effects

MSR-based scaffolds (5 mg MSRs) containing OVA, GM-CSF, and CpG-ODN were then examined for their ability to function as vaccines. Cell recruitment to vaccine scaffolds, compared with blank MSR scaffolds, at different time points was analyzed first. The total number of cells recruited to both systems increased over time, but the vaccine MSR scaffold held 1.8- and 6.5 fold higher numbers of cells at day 5 and 7, respectively, than blank MSR scaffold (Fig. 4a). Further analysis of the cell composition revealed that the recruited cells in the MSR-vaccine consisted mainly of $CD11c^+$ DCs (10%), $B220^+$ B cells (21%), and $CD14^+$ monocytes (52%) (Supplementary Fig. 9). $CD11c^+$ DCs increased over time, and ~4–6-fold higher numbers were observed than in blank MSR scaffolds (Fig. 4b). The level of GM-CSF in the tissue between 1 mm and 3 mm from the injection site was also analyzed, to confirm GM-CSF release *in vivo* (Fig. 4c). Higher GM-CSF levels were maintained for over a week, compared to delivery of blank MSR particles.

The ability of assembled MSRs to allow recruited DCs to process antigen, subsequently traffic to the draining lymph nodes (dLN), and to interact with other immune cells, was then analyzed. Mice were initially immunized with MSR containing only OVA* or both OVA* and GM-CSF. Seven days after injection, the cells in dLN were extracted and analyzed. Delivery of the antigen alone in the MSR scaffold resulted in a slight increase in the number

of AF647$^+$ CD11c$^+$ DCs in the dLN, while with the addition of GM-CSF, the number was drastically increased (Fig. 4d). Including CpG with the GM-CSF and OVA* in the MSR scaffold further increased the number of CD11c$^+$ CD86$^+$ activated DCs in the dLN, compared to MSR releasing only GM-CSF and antigen (Fig. 4e). To test the ability of recruited DCs to process antigen at the site of vaccination and traffic to the dLN, MSRs were loaded with 300 μg of OVA, and the presence of DCs in the dLN presenting OVA257–264 peptide (SIINFEKL) on the major histocompatibility complex I (MHC I) was analyzed 7 days after injection. The MSR vaccine was capable of generating a significant number of SIINFEKL-MHC I$^+$ CD11c$^+$ DCs in the dLN (Fig. 4f and Supplementary Fig. 10).

To test the ability of the MSR-primed DCs to interact with other immune cells in the dLN, mice were again immunized and the dLNs were harvested and analyzed for formation of a germinal center (GC) where immature B cells with antigenic information undergo affinity maturation and somatic hypermutation to generate specific antibody producing plasma B cells[31]. MSR with OVA alone, and the full MSR vaccine both elicited strong GC formation, in an OVA dose-dependent manner (Fig. 4g and Supplementary Fig. 11), indicating that the antigen-presenting DCs exert downstream effects on the B cells in the dLN. Taken together, these data suggest that the MSR vaccine is able to recruit DCs, program them with danger signal while loading them with antigen, and enhance their trafficking to the dLN to present processed antigen to other immune cells.

MSR vaccine generates potent adaptive immune responses

Finally, the ability of the MSR vaccine to induce antigen specific adaptive immune responses was studied. A single immunization with MSRs loaded with OVA, GM-CSF and CpG elicited strong and durable titers of sera anti-OVA IgG_{2a} (Fig. 5a) and IgG_1 (Fig. 5b), indicative of T_H1 and T_H2 responses, respectively. Notably, immunization with MSRs loaded with only OVA elicited a strong antibody response as well, but the response was primarily skewed towards a T_H2 response. By contrast, vaccination with equivalent amounts of GM-CSF, CpG-ODN and OVA as delivered by the MSR, but in bolus form instead, only elicited a moderate and T_H1 skewed response that soon decreased after 100 days. Vaccination with bolus OVA alone led to minimal antibody generation, as expected.

To further characterize the T_H1 and T_H2 responses elicited by MSRs loaded with OVA (MSR + OVA) and the MSR vaccine, we analyzed the production of IFN-γ, a key T_H1 cytokine, and IL-4, a key T_H2 cytokine, after co-culture of the spleen CD4$^+$ T cells (isolated at day 10 post vaccination) with OVA323-339 peptide-pulsed BMDCs (Supplementary Fig. 12). MSR+OVA and the full MSR vaccine showed equally high production of IFN-γ, indicating that the MSR scaffold is capable of driving a strong immune-stimulatory response against OVA. However, the MSR+OVA condition resulted in significantly higher IL-4 production as compared to the MSR vaccine. Taken together, CD4$^+$ T cells primed by the MSR+OVA had a lower IFN-γ to IL-4 ratio, which could explain the observation that the MSR vaccine leads to high levels of both IgG_{2a} and IgG_1 serum antibodies, whereas the MSR+OVA formulation was only able to elicit a strong IgG_1 serum antibody.

To compare the MSR vaccine with a conventional adjuvant vaccine using a prime followed by boost strategy, animals were vaccinated with bolus OVA, bolus vaccine formulation

(GM-CSF + CpG + OVA), Imject Alum with OVA, MSR with OVA, and the MSR vaccine formulation on day 0, and boosted with the same formulations on day 30. We collected serum biweekly or weekly and measured serum IgG_{2a} (Fig. 5c) and IgG_1 (Fig. 5d) antibody against OVA. MSR vaccine resulted in the highest IgG_1 and IgG_{2a} titers as compared with all other groups after primary vaccination. Boosting further increased antibody production in all conditions. Boosting increased the anti-OVA IgG_{2a} level resulting from the bolus vaccine formulation to a similar level as that induced by the first injection of the MSR vaccine (Fig. 5d). This suggests that the MSR vaccine is a potent platform to induce high serum antibody titers and has potential as a single-shot vaccine technology.

Strong humoral responses are highly dependent on the action of $CD4^+$ T follicular helper (T_{FH}) cells[32]. Therefore, we investigated whether the MSR vaccine induced the differentiation of antigen specific T_{FH} cells. Following vaccination with MSRs containing OVA, MSRs containing lysozyme as a negative control, and the full MSR vaccine, 5-(6)-carboxyfluorescein diacetate succinimidyl ester (CFSE) stained $Thy1.2^+$ splenocytes from OT-II mice were adoptively transferred into Thy 1.1^+ C57Bl/6 mice. The $CD4^+$ T cells in OT-II mice have T cell receptors that specifically recognize a sequence on the OVA protein. Four days after immunization, the dLN and spleens were harvested, and the transferred Thy 1.2^+ cells were analyzed. Mice immunized with the full MSR vaccine or MSR loaded with OVA showed significant proliferation of $Thy1.2^+$ $CD4^+$ T cells (Fig. 5e), and generated a significant $CD4^+$ $CXCR5^+$ T helper cell clonal expansion (Fig 5f) and T_{FH} differentiation, whereas mice vaccinated with lysozyme as antigen did not. Together, these data suggest the MSRs have the ability to incorporate and release a variety of factors to induce both T_H1 and T_H2 responses.

To further investigate if the MSR vaccine can enhance $CD8^+$ cytotoxic T lymphocyte (CTL) immune responses, C57Bl/6 mice were immunized with the full MSR vaccine. Seven days after immunization, the strength of the $CD8^+$ T cell response was probed by analyzing the frequency of $tetramer^+$ $CD8^+$ T cells and intracellular IFN-γ^+ $CD8^+$ T cells in the spleen. High numbers of $tetramer^+$ $CD8^+$ T cells (Fig. 5g and Supplementary Fig. 13) and IFN-γ secreting $CD8^+$ T cells (Fig. 5h) were found in the spleens of vaccinated mice. To evaluate antigen-specific $CD8^+$ T cell expansion *in vivo*, CFSE-stained splenocytes isolated from OT-I transgenic mouse were adoptively transferred into naïve mice, and mice immunized with the MSR-vaccine. $CD8^+$ CTL T cells in OT-I mice have a transgenic T cell receptor designed to recognize SIINFEKL-MHC I complex expressed on antigen presenting cells. Seven days after adoptive transfer of CFSE-stained OT-I T cells, the cells in LNs and spleen were retrieved from the recipient mice and CFSE fluorescence was analyzed by flow cytometry. The intensity of the CFSE fluorescence was measured as an indicator of T-cell proliferation, revealing that OT-I T cells proliferated substantially both in LNs and spleen of vaccinated mice (Fig. 5i). These data indicate immunization with the MSR-vaccine induces antigen specific cellular responses that result in T cell proliferation in response to the antigenic information.

To demonstrate one possible application of this approach, we investigated its effect in generating prophylactic tumor protection. Mice were immunized with MSR vaccines or controls, and subsequently challenged with a subcutaneous injection of EG7.OVA

lymphoma cells. MSR vaccines containing CpG-ODN, GM-CSF and OVA were found to delay the onset of tumor growth compared to bolus delivery of the same immune stimulatory agents, a mimic of conventional vaccination (Fig. 5j). MSRs containing OVA (MSR + OVA) suppressed tumor growth in the early stage, but differences over the control condition were lost with time. A bolus vaccine (GM + CpG + OVA 150 μg) resulted in tumor initiation at a similar time point (day 7) as naïve mice, but delayed tumor growth significantly. Tumor growth was much more delayed upon injection of MSR vaccines loaded with 50 μg or 150 μg of OVA. Tumor growth was first observed on day 21, and tumor volume was significantly less than the other conditions at all-time points. The corresponding survival rate also supports the potential utility of the current MSR strategy for prophylactic cancer vaccines (Fig. 5k).

DISCUSSION

This study demonstrates that MSRs are capable of forming, *in situ*, macroporous structures that provide a 3D microenvironment for housing and modulating large numbers of immune cells *in vivo*. Although there has been past work to assemble DNA, peptides, and nanoparticles, the resulting structures were limited to nanostructures for drug delivery or microstructures for *in vitro* cell culture[33]. In this study the interparticle macropores formed by mesoporous silica microparticles could hold host cells. This approach eliminates the need for *ex vivo* construction of a predefined 3D scaffold and brings the assembly process *in vivo*. Although the current microparticles create random pore structures, designing molecular interactions between microparticles could allow self-assembly into a pre-designed, macroporous structure *in vivo*. In addition to cell recruitment, the structure of the MSRs could alter various aspects of cellular phenotype, including cytoskeletal architecture, and differentiation and proliferation[34].

The number of cells within MSR scaffolds is strikingly higher than the number previously reported to be recruited to preformed macroporous polymer scaffolds[3,4]. Generating interparticle macropores using high-aspect-ratio MSRs appears to be crucial to cell number, and the ability of resident cells to reorganize the particles may generate space for additional cell infiltration. The innate immune response to silica likely also contributed to the infiltration of high numbers of host immune cells. Particulates such as silica crystal[35], crystals of monosodium urate (MSU)[36] and aluminum hydroxide (alum)[37] exhibit inflammatory properties, as they are sensed by the cytoplasmic receptor NALP3. Amorphous silica nanoparticles have recently been shown to activate the NALP3 inflammasome as well[38]. Although MSRs used in this system are larger than cells, and are unlikely to be internalized intact, it is possible that smaller particles are produced during their degradation *in vivo* over time and internalized by cells, resulting in NALP3 activation. Surface hydroxyl groups have also been linked to alternative complement activation[39]. We speculate that NALP3 activation and complement binding are likely involved in inflammation resulting from MSRs.

To modulate the recruited host immune cells, sustained release of a small inflammatory molecule (GM-CSF), a ssDNA TLR agonist (CpG-ODN), and a model antigen protein (OVA) was achieved by exploiting the high surface area and pore volume of the MSRs. This

approach prolongs presentation of these molecules in the surrounding tissue, allowing one to modulate DC enrichment, activation and antigen processing, and subsequent homing to lymph nodes. The current release profile is based on diffusion of loaded molecules from the mesopores, but the release rate can be further actively controlled[40,41].

We observe significant enrichment of myeloid DCs in GM-CSF releasing scaffolds, which is likely a combined effect of peripheral DC migration and *in situ* differentiation of DCs from precursors. Prolonged presentation of antigens and adjuvants to immune cells, which is believed to be crucial to enable long-term stimulation of DCs in order to break immune tolerance[42,43], has been demonstrated to yield potent immune responses in past studies[7,44]. MSRs loaded with OVA, GM-CSF, and CpG-ODN were here found to enhance systemic IgG_{2a} and IgG_1 serum antibody levels and CTL responses, compared to bolus vaccine formulations. The induction of these strong humoral and cellular immune responses is likely a result of the high number of DCs, their sustained and prolonged activation and priming, and their subsequent interactions with CD4 and CD8 T cells in the lymph node.

The ability to tune the immune response is one of the advantages of the MSR system. In this study, CpG was used to activate the DCs to secrete T_H1 cytokines and prime $CD8^+$ and $CD4^+$ T cells. The boost of IgG_{2a} antibody response and anti-tumor effect with the MSR vaccine are likely the manifestation of a T_H1 response. Sustained delivery of antigens and adjuvants from the MSRs likely contributes to, though is not solely responsible for, generating high serum antibody titers. Previous reports using polymer nano or microparticles to release antigens and adjuvants[45,46] have led to moderate antibody titers, and required a secondary boost. In contrast, with MSRs, a single prime injection was sufficient to induce antibody titers over 2 orders of magnitude higher than the bolus control, and comparable to a prime-boost using bolus vaccination. Although Alum loaded with OVA and CpG induces high IgG_1 serum antibody titer, it induces lower IgG_{2a} serum titer than bolus formulations composed of OVA and CpG, suggesting it is not effective at inducing a T_H1 skewed immune response[47]. In contrast, the MSR vaccine leads to high levels of both IgG_{2a} and IgG_1 serum antibodies. These results indicate that cell enrichment along with sustained release of antigens and adjuvants plays a key role in driving the potent immune response. The immunoactive nodule generated by the MSR system can likely generate cell-cell and cell-material interactions that are crucial to the development of potent CTL and antibody responses.

This injectable scaffold may provide a useful platform for prophylactic and therapeutic vaccination. The success of the HPV vaccine in cervical cancer has created interest in additional prophylactic opportunities for other types of cancer where individuals at high risk (e.g., breast cancer) can be identified in advance, and tumor antigens common to many patients' or patient specific antigens are being actively identified. The prophylactic tumor vaccine study using MSRs clearly demonstrates that this injectable scaffold system has potential to suppress the growth of tumors. However, the major value of this new technology would likely be as a therapeutic cancer vaccine, and additional studies are required to test its activity in that setting. In addition, the striking serum antibody response induced by this approach is likely relevant to the treatment of viral diseases that are resistant to conventional treatment. The injection site reactions may not be acceptable in situations where an effective

immune response can be generated with conventional vaccine technologies, nor in situations where the disease does not present a significant danger to the patient. However, in diseases that are both life-threatening and resistant to conventional therapy, we do not believe an injection site reaction would be a significant impediment to vaccine use.

The biodegradation and safety of the injected MSRs should be considered for potential medical applications. Mesoporous silica is composed of an amorphous silica which degrades in the body over time[23,24]. Synthetic amorphous silica is generally recognized as safe by the FDA, and is used in cosmetics and as a food additive. The current administration route (subcutaneous injection) and quantity (5 mg) of MSR used in these studies resulted in a significant biodegradation in 28 days, and did not cause severe local inflammation, side effects, or animal mortality, indicative of the biocompatibility of this technology. This is obviously in contrast with another type of fibrous silica, asbestos, which is a crystalline material that does not degrade in the body, and thus acts as a carcinogen. We plan to investigate the *in vivo* degradation of MSRs and associated duration of inflammation in more depth in the future.

Looking forward, the physicochemical properties of MSRs could be further tuned, including the coupling of surface ligands, to enhance their capability to modulate cell behavior. This system could be further applied to other fields, possibly including detection of circulating tumor cells or recruitment of stem cells.

METHODS

Synthesis and characterization of mesoporous silica rods (MSRs)

MSRs were prepared following the previous reports with a slight modification[20,21]. To synthesize high aspect ratio MSRs (88 μm × 4.5 μm), typically, 4 g of P123 surfactant (average M_n ~5800, Aldrich) and 46 mg of ammonium fluoride (NH_4F, 98%, sigma-aldrich) were dissolved in 150 g of 1.6 M HCl solution and were stirred with 8.6 g of tetraethyl orthosilicate (TEOS, 98%, Aldrich) at 40 °C for 20 h, followed by aging at 100 °C for 24 h. To prepare lower aspect ratio MSRs (37 μm × 3.2 μm), the synthesis is conducted without adding ammonium fluoride. To extract the surfactant, the as synthesized particles were refluxed for 10 h in 1% HCl in ethanol. The resulting MSR particles were then filtered, washed with ethanol, and dried. MSR morphology was measured using optical microscopy, SEM, and TEM. Pore size, pore volume and surface area were analyzed using N_2 adsorption/desorption isotherms. The pore filled MSRs were prepared following a previous report with a slight modification[48]. One gram of high aspect ratio MSRs was impregnated with 1.4 mL of TEOS under gentle agitation. Aqueous HCl (pH 1) was added dropwise and mixed with MSRs. The mixture powder was aged at 40 °C for 3 h and water and ethanol formed during hydrolysis were removed by evaporation at 80 °C. The impregnation procedure was repeated 4 times. The monolith-type MSRs were prepared by pressing 5 mg of high aspect ratio MSRs in a mold of 8 mm diameter using a laboratory press.

Bone Marrow Derived Dendritic Cell (BMDC) isolation and culture

BMDC were derived using standard techniques[49,50]. In brief, bone marrow cells were isolated from female C57Bl/6J mice (Jackson Laboratories) and cultured in RPMI based media (Lonza) supplemented with 10% heat inactivated FBS (Sigma-Aldrich), 1% penicillin/streptomycin, 50μM β-mercaptoethanol and 20 ng/ml GM-CSF (Peprotech). Dendritic cells were harvested and used for experiments between day 7 and 10 of differentiation. Differentiation was confirmed using the CD11c, CD11b and MHC II surface markers.

In vitro release study

1 μg of GM-CSF was loaded onto 5 mg of MSRs for 8 h at room temperature under vigorous shaking. The MSRs were then lyophilized and reconstituted in release media composed of RPMI supplemented with 1% penicillin/ streptomycin and 1% heat-inactivated FBS). Supernatant containing released GM-CSF was collected periodically. The release of GM-CSF was measured in two different ways; by measuring radioactivity in release media using radio-labeled GM-CSF (^{125}I-GM-CSF) or by enzyme-linked immunosorbent assay (ELISA) using incorporation of normal (non-radioactive) GM-CSF, in order to investigate the release of bioactive GM-CSF. The amount of ^{125}I-GM-CSF released was determined at each time point by counting the radioactivity of the collected media in a gamma counter. Bioactive GM-CSF levels in the collected media were measured using ELISA (R&D systems). To examine the *in vitro* release of CpG-ODN, 100 μg of CpG-ODN (Oligofactory) was loaded onto 5 mg of MSRs at room temperature for 8 h under vigorous shaking, and MSRs were subsequently lyophilized and redispersed in 1% BSA. Release media was collected periodically, and the concentration of CpG-ODN was measured with the OliGreen ssDNA Assay (Invitrogen) according to manufacturer's protocol. Similarly, to examine the *in vitro* release of ovalbumin, 300 μg of ovalbumin (Sigma Aldrich) was loaded onto 5 mg of MSRs, lyophilized and redispersed in PBS. Release media was collected periodically, and the ovalbumin concentration was determined using a micro-BCA Protein Assay (Pierce). All release studies were done in 37°C under moderate shaking.

Subcutaneous injection with MSR scaffolds

Typically 5 mg of blank MSRs or MSRs loaded with bioactive agents, recombinant murine GM-CSF (Peprotech 315-03), CpG-ODN (Invivogen vac-1826-1), or OVA (Invivogen vac-pova), suspended in cold PBS (150 μl) were injected subcutaneously into the flank of female C57Bl/6J mice using an 18-gauge needle.

Confocal analysis

Animals were injected with MSRs containing with OVA conjugated with Alexa Fluoro 488 (AF488). At various time points, the scaffolds were explanted, and fixed in neutral buffered formalin at 4 °C overnight. Scaffolds were then embedded in OCT. Frozen sections of the scaffolds were stained with rhodamine-phalloidin (Biotium) and DAPI (Life Technologies) and visualized using a Zeiss LSM 710 confocal microscope.

MSR nodule measurement

Animals were injected with 5 mg of blank MSRs. Subcutaneous nodule size was quantified over time by measuring the nodule length, width and height using a caliper.

Histology analysis

Animals were injected with MSR with 1 μg GM-CSF and the scaffold was explanted on day 3 and 7 post injection. Scaffolds were paraffin embedded, sectioned and stained with Hematoxylin and eosin.

Preparation of MSR vaccine and immunization

5 mg of MSRs were loaded with 1 μg of GM-CSF, 100 μg of CpG-ODN and OVA (50, 150, or 300 μg) for 12 h at room temperature under vigorous shaking. The particles were then lyophilized, resuspended in cold PBS (150 μl) and injected subcutaneously into the flank of female C57Bl/6J mice.

Cell isolation from MSR scaffolds explanted from animals

Scaffolds were excised at various time points. The tissues were processed through mechanical disruption and suspended in cold PBS. The cell suspension was then filtered through a 40 μm cell strainer to isolate the cells from the larger sized MSRs. The cells and small remaining MSR particles were pelleted, washed with cold PBS, and counted. The portion of cells in the mixture of cells and small silica particles was accessed in SSC and FSC gating in flow cytometry (BD LSRII) (Supplementary Fig. 14). Based on the counts from Coulter counter and the percentage of cells determined from FACS gating, the number of live cells in the MSR scaffolds could be calculated.

Analysis of DC recruitment to MSR scaffolds and their emigration to lymph nodes

APC-conjugated CD11c (eBioscience 17–0114), FITC-conjugated CD11b (eBioscience 11–0112) stains were conducted for DC and leukocyte recruitment analysis, and APC-conjugated CD11c, FITC-conjugated MHC II (eBioscience 11–5332), and PE-conjugated CD86 (eBioscience 12–0862) stains were conducted for DC maturation analysis. Cells were gated according to positive FITC, APC and PE using isotype controls, and the percentages of cells staining positive for each surface antigen were recorded. To track DC emigration to lymph nodes (LNs), OVA labeled with Alexa Fluor 647 was loaded in MSRs and injected subcutaneously. The inguinal lymph nodes were harvested at 7 days post injection. Cell suspensions from LNs were prepared by mechanical disruption and pressing of the tissue through 40 μm cell strainers, and examined for $CD11c^+$ $AF647^+$ cell numbers by flow cytometry. All flow cytometry antibodies were diluted according to the manufacturer's suggestions.

In vivo cytokine analysis

Tissue samples between 1 mm and 3 mm from the scaffold were extracted from the animals and digested using the Tissue Protein Extraction (T-Per) Reagent (Pierce), and homogenized via brief sonication. Cell debris was pelleted with centrifugation. The supernatant was analyzed using Bio-Plex Pro™ mouse cytokine 23-plex immunoassay (Bio-Rad

M60009RDPD) and ELISA (R&D systems DY415), according to the manufacturer's instructions.

Detection of SIINFEKL presenting DCs in the draining lymph node (dLN)

To analyze OVA257–264 (SIINFEKL) peptide (Anaspec) presenting DCs, dLNs were isolated and digested on day 7 post vaccination. dLN cells were enumerated and stained with APC conjugated anti-mouse CD11c (eBioscience 17–0114) and PE conjugated anti-mouse SIINFEKL peptide bound to H-2Kb (eBioscience 12–5743) for 15 minutes on ice. Cells were washed and assessed by flow cytometry.

Detection of germinal center formation

To analyze GC formation, dLNs were isolated on day 7 post vaccination. Cells were enumerated, stained with FITC conjugated anti-mouse B220 (eBioscience 11–0452) and APC conjugated anti-mouse GL7 (eBioscience 51–5902) for 15 minutes on ice. Cells were washed and assessed by flow cytometry.

Detection of OVA-specific humoral responses

Animals were vaccinated with bolus 300 μg OVA (bolus OVA), bolus vaccine containing 300 μg OVA, 100 μg CpG-ODN and 1 μg GM-CSF (bolus vaccine), 5 mg MSR containing 300 μg OVA (MSR + OVA), and MSR vaccine containing 5 mg MSRs, 300 μg OVA, 100 μg CpG-ODN and 1 μg GM-CSF (MSR vaccine). Blood sera were collected once every 14 days. Sera were then analyzed for IgG_1 and IgG_{2a} antibodies against ovalbumin using ELISA (Biolegend 406603 and Biolegend 407104, respectively). High affinity plates were coated using OVA (Invivogen vac-pova) and anti-OVA titers were defined as the lowest serum dilution at which the ELISA OD reading was equal to OD value 0.3[65]. In the booster experiments, animals were vaccinated on day 0 with bolus OVA, bolus vaccine, Imject Alum (Pierce) loaded with 300 μg OVA (Alum + OVA), MSR + OVA, and MSR vaccine, and re-vaccinated on day 30 with the same formulations. Imject Alum was loaded with OVA according to the manufacturer's protocol.

$CD4^+$ T cell cytokine secretion assay

The spleens of the animals were isolated and digested at day 10 post vaccination. $CD4^+$ T cells were magnetically sorted from each spleen (Miltenyi Biotec). The T cells were then co-cultured with LPS (100 ng/ml)-primed DCs pulsed with 1 μM OVA323-339 peptide (Invivogen) for 24 hours in round bottom 96 well plates. $CD4^+$ T cells and DCs were co-cultured at the ratio of 2 to 1 (T to DC). Media was collected after 24 hours and analyzed for IL-4 and IFN-γ using ELISA (eBioscience 88–7711).

OVA-specific $CD4^+$ T cell expansion and follicular helper T-cell analysis

Recipient Thy 1.1^+ mice were vaccinated subcutaneously with 5 mg MSRs containing 300 μg OVA, 5 mg MSRs containing 300 μg lysozyme, or MSR vaccine containing 5 mg MSRs, 300 μg OVA, 100 μg CpG-ODN and 1 μg GM-CSF. On day 3, 2×10^7 splenocytes were isolated from donor OT-II (Thy 1.2^+) mice, labeled with CFSE and adoptively transferred i.v. into the recipient vaccinated mice. On day 7, recipient mice were sacrificed, and dLN

and spleens were isolated. Cells were analyzed for Thy1.2$^+$ CD4$^+$ (eBiosciences 17–0902, eBioscience 25–0041, respectively) T cell expansion, and Thy1.2$^+$ CD4$^+$ CXCR5$^+$ (eBiosciences 12–1851) follicular helper T-cells using flow cytometry.

OVA-specific CD8+ T cell expansion analysis

Recipient mice were vaccinated subcutaneously with 5 mg MSRs containing 5 mg MSRs, 300 μg OVA, 100 μg CpG-ODN and 1 μg GM-CSF. On day 3, 2 ×10^7 splenocytes were isolated from donor OT-I mice, labeled with CFSE and adoptively transferred i.v. into the recipient vaccinated mice. Seven days following transfer, recipient mice were sacrificed, and dLN and spleens were isolated and analyzed for CD3$^+$ CD8$^+$ (eBioscience 25–0031, eBioscience 17–0081, respectively) T cell expansion.

Prophylactic tumor study

Animals were immunized with 5 mg MSRs containing 150 μg OVA (MSR + OVA), MSR vaccine containing 5 mg MSRs, 150 μg or 50 μg OVA, 100 μg CpG-ODN and 1 μg GM-CSF (MSR vaccine), and bolus vaccine containing 150 μg OVA, 100 μg CpG-ODN and 1 μg GM-CSF (Bolus vaccine). After 10 days, animals were challenged with a subcutaneous injection of 1 × 10^6 EG7.OVA lymphoma cells (ATCC) in the back of the neck. Tumor growth was monitored by measuring the tumor length, width and height. Animals were euthanized for humane reasons when tumors grew to 20 mm in longest diameter.

Animal protocol

All animal studies were performed in accordance with NIH guidelines, under approval of Harvard University's Institutional Animal Care and Use Committee.

Statistical analysis

All values in the present study were expressed as mean ± S.D with the exception of Fig. 5j, which is expressed as mean ± SEM. Sample sizes were calculated, using InStat software, to allow the statistical significance of differences of 50% or greater to be determined. The specific sample size required depended on the experiment. Statistical analysis was performed using GraphPad Prism and Microsoft Excel. Sample variance was tested using the F test. For samples with equal variance, the significance between the groups were analyzed by a, two-tailed, student's t test. For samples with unequal variance, a two tailed Welch's t-test was performed. In all cases, a P value of less than 0.05 was considered significant.

Supplementary Material

Refer to Web version on PubMed Central for supplementary material.

ACKNOWLEDGEMENTS

This work was supported by the NIH (1R01EB015498), the NSF GRFP, the Wyss Institute for Biologically Inspired Engineering at Harvard University, and NRF grants (2012R1A1A1042735, 2010-0027955) funded by the National Research Foundation under the Ministry of Science, ICT & Future Planning, Korea. We also thank DF/HCC Research Pathology Core and Dr. Roderick Bronson for the examination of the histology slides and Dr. James Weaver from the Wyss Institute of Biologically Inspired Engineering for his help with scanning electron

microscopy (SEM). Lastly, we thank Professor Rebecca Betensky from the Department of Biostatistics, Harvard School of Public Health and the Harvard Catalyst for her help with statistical analysis; Harvard Catalyst is supported, in part, by the NIH (UL1 TR001102).

REFERENCES

1. Jähnisch H, et al. Dendritic cell-based immunotherapy for prostate cancer. Clin. Dev. Immunol. 2010; 2010:1–8.
2. Porter DL, Levine BL, Kalos M, Bagg A, June CH. Chimeric antigen receptor-modified T cells in chronic lymphoid leukemia. N. Engl. J. Med. 2011; 365:725–733. [PubMed: 21830940]
3. Ali OA, Huebsch N, Cao L, Dranoff G, Mooney DJ. Infection-mimicking materials to program dendritic cells in situ. Nat. Mater. 2009; 8:151–158. [PubMed: 19136947]
4. Ali OA, Emerich D, Dranoff G, Mooney DJ. In situ regulation of DC subsets and T cells mediates tumor regression in mice. Sci. Transl. Med. 2009; 1 8ra19.
5. Stephan MT, Moon JJ, Um SH, Bershteyn A, Irvine DJ. Therapeutic cell engineering with surface-conjugated synthetic nanoparticles. Nat. Med. 2010; 16:1035–1041. [PubMed: 20711198]
6. Moon JJ, et al. Interbilayer-crosslinked multilamellar vesicles as synthetic vaccines for potent humoral and cellular immune responses. Nat. Mater. 2011; 10:243–251. [PubMed: 21336265]
7. John ALS, Chan CY, Staats HF, Leong KW, Abraham SN. Synthetic mast-cell granules as adjuvants to promote and polarize immunity in lymph nodes. Nat. Mater. 2012; 11:250–257. [PubMed: 22266469]
8. Park J, et al. Combination delivery of TGF-β inhibitor and IL-2 by nanoscale liposomal polymeric gels enhances tumour immunotherapy. Nat. Mater. 2012; 11:895–905. [PubMed: 22797827]
9. Engelmayr GC, et al. Accordion-like honeycombs for tissue engineering of cardiac anisotropy. Nat. Mater. 2008; 7:1003–1010. [PubMed: 18978786]
10. Freed LE, et al. Biodegradable polymer scaffolds for tissue engineering. Nat. Biotechnol. 1994; 12:689–693.
11. Place ES, George JH, Williams CK, Stevens MM. Synthetic polymer scaffolds for tissue engineering. Chem. Soc. Rev. 2009; 38:1139–1151. [PubMed: 19421585]
12. Lutolf M, Hubbell J. Synthetic biomaterials as instructive extracellular microenvironments for morphogenesis in tissue engineering. Nat. Biotechnol. 2005; 23:47–55. [PubMed: 15637621]
13. Yamada Y, et al. Autogenous injectable bone for regeneration with mesenchymal stem cells and platelet-rich plasma: tissue-engineered bone regeneration. Tissue Eng. 2004; 10:955–964. [PubMed: 15265313]
14. Yuen WW, Du NR, Chan CH, Silva EA, Mooney DJ. Mimicking nature by codelivery of stimulant and inhibitor to create temporally stable and spatially restricted angiogenic zones. Proc. Natl. Acad. Sci. USA. 2010; 107:17933–17938. [PubMed: 20921366]
15. Xia T, et al. Polyethyleneimine coating enhances the cellular uptake of mesoporous silica nanoparticles and allows safe delivery of siRNA and DNA constructs. ACS nano. 2009; 3:3273–3286. [PubMed: 19739605]
16. Kim J, et al. Multifunctional uniform nanoparticles composed of a magnetite nanocrystal core and a mesoporous silica shell for magnetic resonance and fluorescence imaging and for drug delivery. Angew. Chem. Int. Ed. 2008; 47:8438–8441.
17. Li Z, Barnes JC, Bosoy A, Stoddart JF, Zink JI. Mesoporous silica nanoparticles in biomedical applications. Chem. Soc. Rev. 2012; 41:2590–2605. [PubMed: 22216418]
18. Garcia-Bennett AE. Synthesis, toxicology and potential of ordered mesoporous materials in nanomedicine. Nanomedicine. 2011; 6:867–877. [PubMed: 21793677]
19. Petushkov A, Ndiege N, Salem AK, Larsen SC. Toxicity of silica nanomaterials: Zeolites, mesoporous silica, and amorphous silica nanoparticles. Adv. Mol. Toxicol. 2010; 4:223–266.
20. Zhao D, Huo Q, Feng J, Chmelka BF, Stucky GD. Nonionic triblock and star diblock copolymer and oligomeric surfactant syntheses of highly ordered, hydrothermally stable, mesoporous silica structures. J. Am. Chem. Soc. 1998; 120:6024–6036.
21. Schmidt-Winkel P, Yang P, Margolese DI, Chmelka BF, Stucky GD. Fluoride-induced hierarchical ordering of mesoporous silica in aqueous acid-syntheses. Adv. Mater. 1999; 11:303–307.

22. Hudson SP, Padera RF, Langer R, Kohane DS. The biocompatibility of mesoporous silicates. Biomaterials. 2008; 29:4045–4055. [PubMed: 18675454]
23. He Q, Shi J, Zhu M, Chen Y, Chen F. The three-stage in vitro degradation behavior of mesoporous silica in simulated body fluid. Microporous Mesoporous Mater. 2010; 131:314–320.
24. Cauda V, Schlossbauer A, Bein T. Bio-degradation study of colloidal mesoporous silica nanoparticles: effect of surface functionalization with organo-silanes and poly (ethylene glycol). Microporous Mesoporous Mater. 2010; 132:60–71.
25. Dieu M, et al. Selective recruitment of immature and mature dendritic cells by distinct chemokines expressed in different anatomic sites. J. Exp. Med. 1998; 188:373–386. [PubMed: 9670049]
26. Randolph GJ, Ochando J, Partida-Sánchez S. Migration of dendritic cell subsets and their precursors. Annu. Rev. Immunol. 2008; 26:293–316. [PubMed: 18045026]
27. Steinman RM. The dendritic cell system and its role in immunogenicity. Annu. Rev. Immunol. 1991; 9:271–296. [PubMed: 1910679]
28. Banchereau J, Steinman RM. Dendritic cells and the control of immunity. Nature. 1998; 392:245–252. [PubMed: 9521319]
29. Medzhitov R, Janeway CA Jr. Innate immunity: impact on the adaptive immune response. Curr. Opin. Immunol. 1997; 9:4–9. [PubMed: 9039775]
30. Klinman DM. Immunotherapeutic uses of CpG oligodeoxynucleotides. Nat. Rev. Immunol. 2004; 4:249–259. [PubMed: 15057783]
31. Victora GD, Nussenzweig MC. Germinal centers. Annu. Rev. Immunol. 2012; 30:429–457. [PubMed: 22224772]
32. Crotty S. Follicular Helper CD4 T Cells (Tfh). Annu. Rev. Immunol. 2011; 29:621–663. [PubMed: 21314428]
33. Zhang S. Fabrication of novel biomaterials through molecular self-assembly. Nat. Biotechnol. 2003; 21:1171–1178. [PubMed: 14520402]
34. Russell B, Desai TA, Goldspink P. Temporal release of growth factors from 3d micro rod scaffolds for tissue regeneration. EP 2170419 A1 filed 18 Jul. 2008, and issued 7 Apr. 2010
35. Dostert C, et al. Innate immune activation through Nalp3 inflammasome sensing of asbestos and silica. Science. 2008; 320:674–677. [PubMed: 18403674]
36. Sharp FA, et al. Uptake of particulate vaccine adjuvants by dendritic cells activates the NALP3 inflammasome. Proc. Natl. Acad. Sci. USA. 2009; 106:870–875. [PubMed: 19139407]
37. Hornung V, et al. Silica crystals and aluminum salts activate the NALP3 inflammasome through phagosomal destabilization". Nat. Immunol. 2008; 9:847–856. [PubMed: 18604214]
38. Zhang H, et al. Processing pathway dependence of amorphous silica nanoparticle toxicity: colloidal vs pyrolytic. J. Am. Chem. Soc. 2012; 134:15790–15804. [PubMed: 22924492]
39. Reddy ST, et al. Exploiting lymphatic transport and complement activation in nanoparticle vaccines. Nat. Biotechnol. 2007; 25:1159–1164. [PubMed: 17873867]
40. Meng H, et al. Autonomous in vitro anticancer drug release from mesoporous silica nanoparticles by pH-sensitive nanovalves. J. Am. Chem. Soc. 2010; 132:12690–12697. [PubMed: 20718462]
41. Yang P, Shili G, Jun L. Functionalized mesoporous silica materials for controlled drug delivery. Chem. Soc. Rev. 2012; 41:3679–3698. [PubMed: 22441299]
42. Zou W. Immunosuppressive networks in the tumour environment and their therapeutic relevance. Nat. Rev. Cancer. 2005; 5:263–274. [PubMed: 15776005]
43. Rabinovich GA, Gabrilovich D, Sotomayor EM. Immunosuppressive strategies that are mediated by tumor cells. Annu. Rev. Immunol. 2007; 25:267. [PubMed: 17134371]
44. Moon JJ, et al. Enhancing humoral responses to a malaria antigen with nanoparticle vaccines that expand Tfh cells and promote germinal center induction. Proc. Natl. Acad. Sci. USA. 2012; 109:1080–1085. [PubMed: 22247289]
45. Zhang XQ, et al. Potent antigen-specific immune responses stimulated by codelivery of CpG ODN and antigens in degradable microparticles. J. Immunother. 2007; 30:469–478. [PubMed: 17589287]

46. Uto T, et al. The induction of innate and adaptive immunity by biodegradable poly (γ-glutamic acid) nanoparticles via a TLR4 and MyD88 signaling pathway. Biomaterials. 2011; 32:5206–5212. [PubMed: 21492934]

47. Hutchison S, et al. Antigen depot is not required for alum adjuvanticity. FASEB J. 2012; 26:1272–1279. [PubMed: 22106367]

48. Lu A, Schmidt W, Spliethoff B, Schüth F. Synthesis and Characterization of Nanocast Silica NCS-1 with CMK-3 as a Template. Chem. Eur. J. 2004; 10:6085–6092. [PubMed: 15515070]

49. Faulkner L, Buchan G, Baird M. Interleukin-10 does not affect phagocytosis of particulate antigen by bonemarrow-derived dendritic cells but does impair antigen presentation. Immunology. 2000; 99:523–531. [PubMed: 10792499]

50. Bhattacharya P, Gopisetty A, Ganesh BB, Sheng JR, Prabhakar BS. GM-CSF-induced, bone-marrow-derived dendritic cells can expand natural Tregs and induce adaptive Tregs by different mechanisms. J. Leukoc. Biol. 2011; 89:235–249. [PubMed: 21048215]

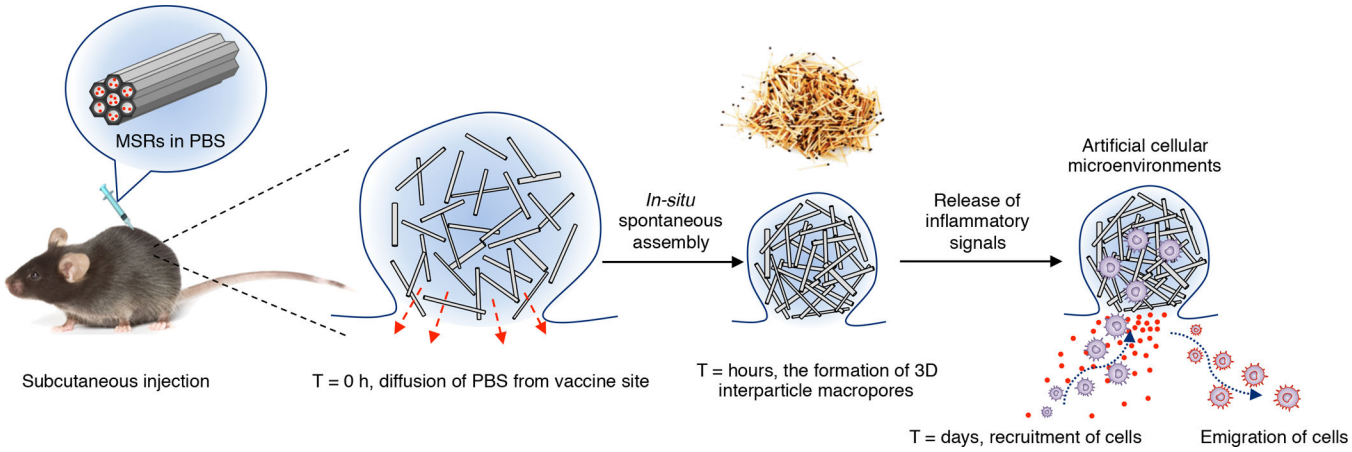

Figure 1. A schematic representation of *in vivo* spontaneous assembly of mesoporous silica rods (MSRs) and recruitment of host cells for maturation

A PBS dispersion of MSRs is injected into subcutaneous tissue of mice to form a pocket. After diffusion of PBS from the pocket, *in situ* spontaneous assembly of MSRs, analogous to the random assembly of thrown matchsticks, results in the formation of three-dimensional interparticle spaces where host cells can be recruited and educated by the payloads in MSRs. Educated cells may then emigrate from the structure to interact with other immune cells.

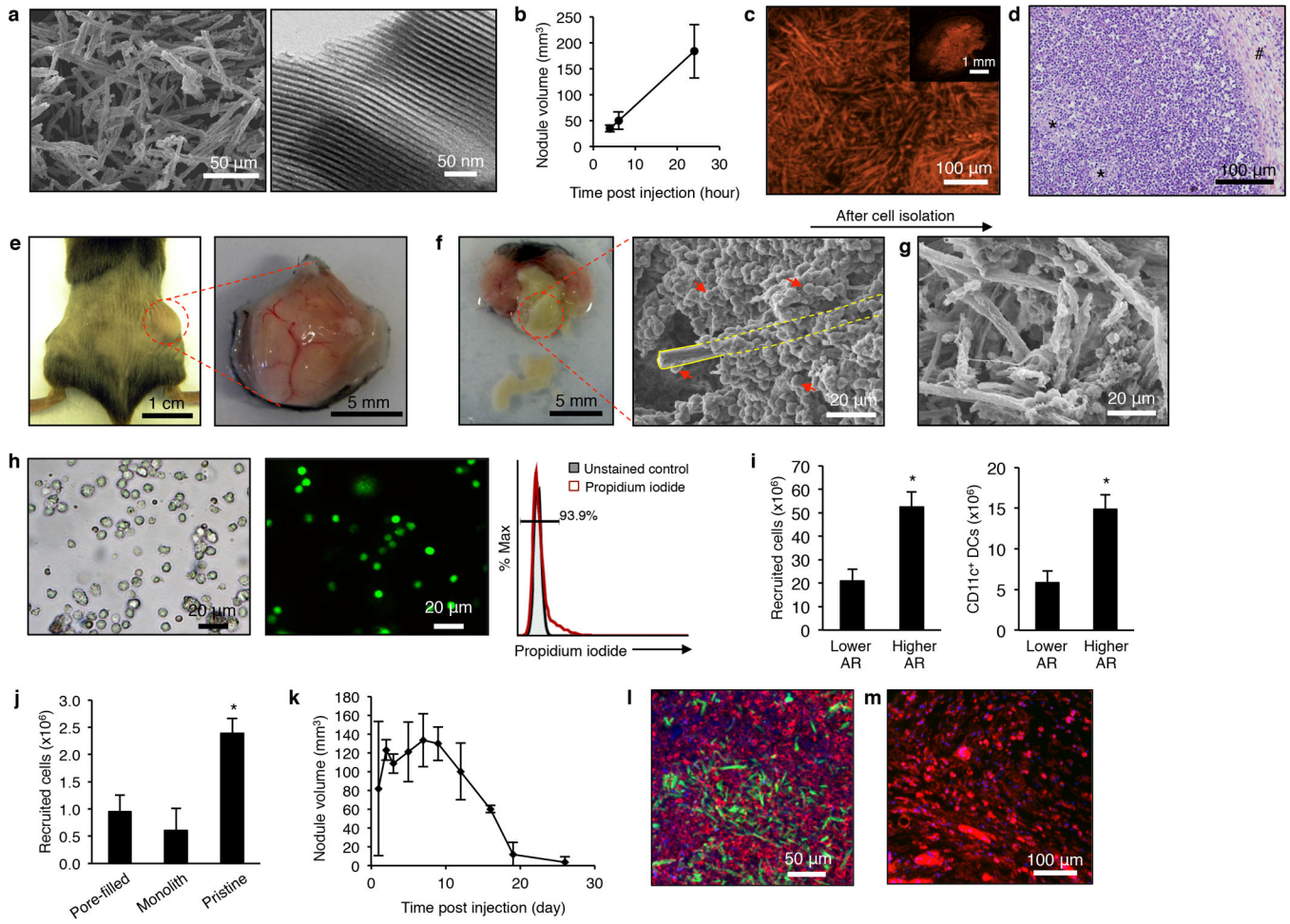

Figure 2. Subcutaneous injection of blank MSRs results in their spontaneous assembly *in vivo* and substantial numbers of cells are recruited into interparticle pores of assembled MSRs

(a) SEM (left) and TEM (right) images of MSRs of 88 μm in length and 4.5 μm in diameter. **(b)** Nodule size measurements after injection of blank MSRs in time course of hours (n=3). **(c)** Fluorescent image of cross-section of the retrieved nodule after injection of rhodamine B-labeled MSRs. **(d)** H&E staining of sectioned nodule retrieved at day 3 after subcutaneous injection. *: representative crosssection of MSRs. #: surrounding fibrotic tissue. **(e)** Localization of MSRs as a nodule in the dorsal flank of a mouse one day after subcutaneous injection (left) and the retrieved nodule (right). **(f)** Isolation of MSR-scaffold and cells from the nodule (left) and SEM photomicrograph (right) demonstrating a high number of recruited cells. Yellow outline represents a visible MSR. Red arrows indicate the representative cells. **(g)** SEM image of MSR-scaffold after removal of most recruited cells. **(h)** Representative bright-field optical microscope of the isolated cells (left), fluorescent image of the cells after live-dead staining (middle, green: live cells, red: dead cells), and propidium iodide (PI) flow cytometry analysis of retrieved cells from the nodule (right). **(i)** Number of total recruited cells (left) and $CD11c^+$ DCs (right) into MSRs (20 mg) with lower and higher aspect ratio, respectively, at day 7 post injection (n=3). **(j)** Number of total recruited cells in 5 mg of pore-filled, pressed, and pristine MSRs, respectively, at day 3 post injection (n=4). **(k)** Nodule size measurement after injection of blank MSR in time course

over weeks (n=3). **(l,m)** Confocal images of sectioned nodules retrieved at (l) day 7 and (m) day 28 post-injection, respectively. The injected MSRs were labeled with AF488 and loaded with GM-CSF (1 μg). The cryosections were stained with DAPI and rhodamine-phalloidin. Biological replicates were used and studies were repeated at least 2 times in the lab. Values represent mean and s.d. * represents $p<0.05$.

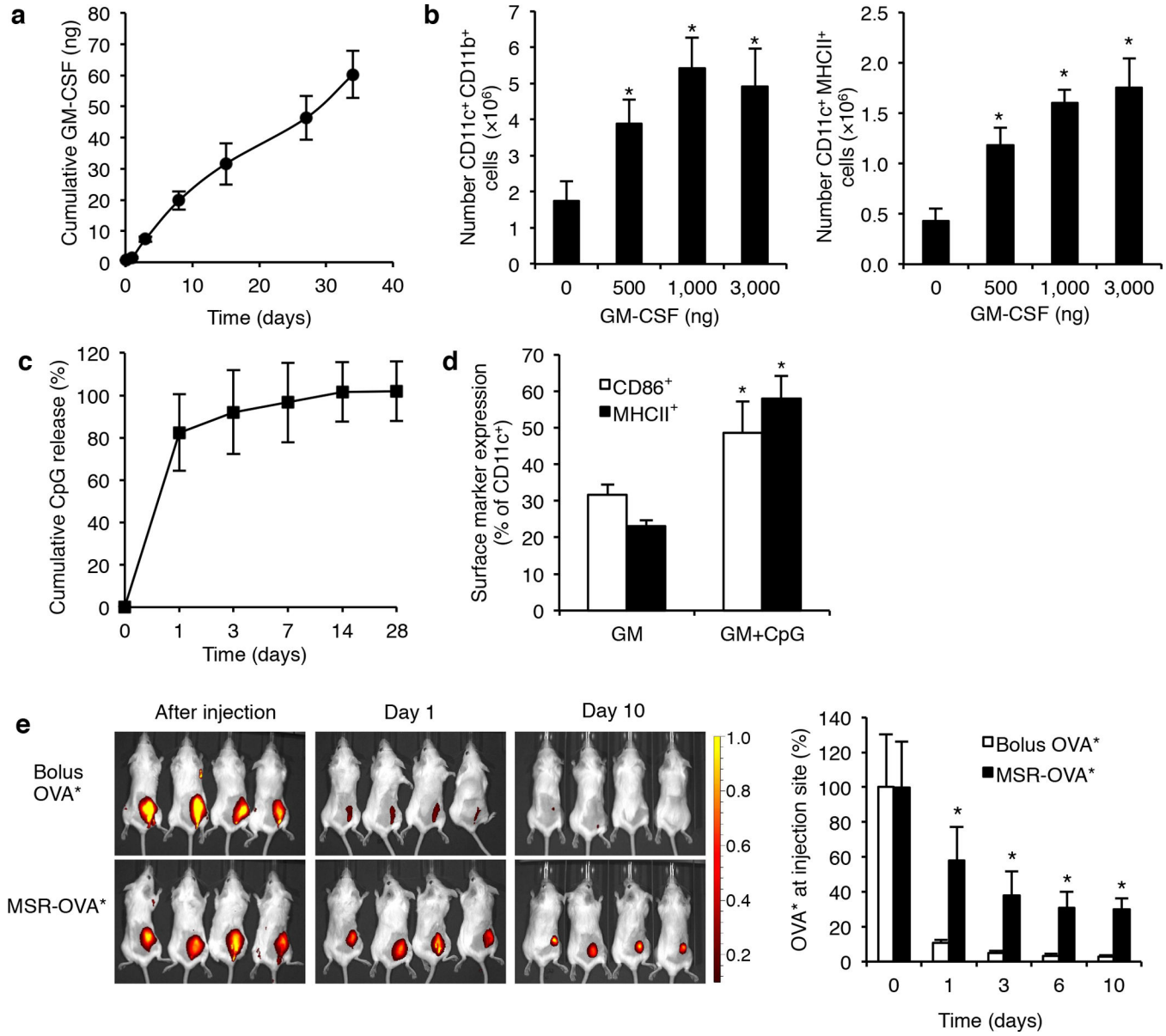

Figure 3. Cytokine, PAMP, and model antigen are released from MSR-scaffold in sustained manner *in vitro* and *in vivo*

(a)*In vitro* level of bioactive GM-CSF released from MSRs analyzed using ELISA. **(b)** Numbers of $CD11c^+$ $CD11b^+$ (left) and $CD11c^+$ MHC II^+ (right) DCs recruited to MSR-scaffold loaded with different amounts of GM-CSF (n=4). **(c)***In vitro* release of CpG from MSRs, as determined using OliGreen ssDNA assay. **(d)** Levels of activation markers (CD86 and MHC II) of recruited $CD11c^+$ DCs with injection of MSRs loaded with GM-CSF, or both GM-CSF and CpG, respectively. (n=4) **(e)** Representative NIR fluorescent images of mice injected with bolus OVA labeled with Alexafluor-647 (OVA*) or MSRs loaded with same amount of OVA* (left), and relative OVA* remaining in injection sites as a function of time, as based on fluorescent imaging (right) (n=4). Biological replicates were used and

studies were repeated at least 2 times in the lab. Values represent mean and s.d. * represents $p<0.05$.

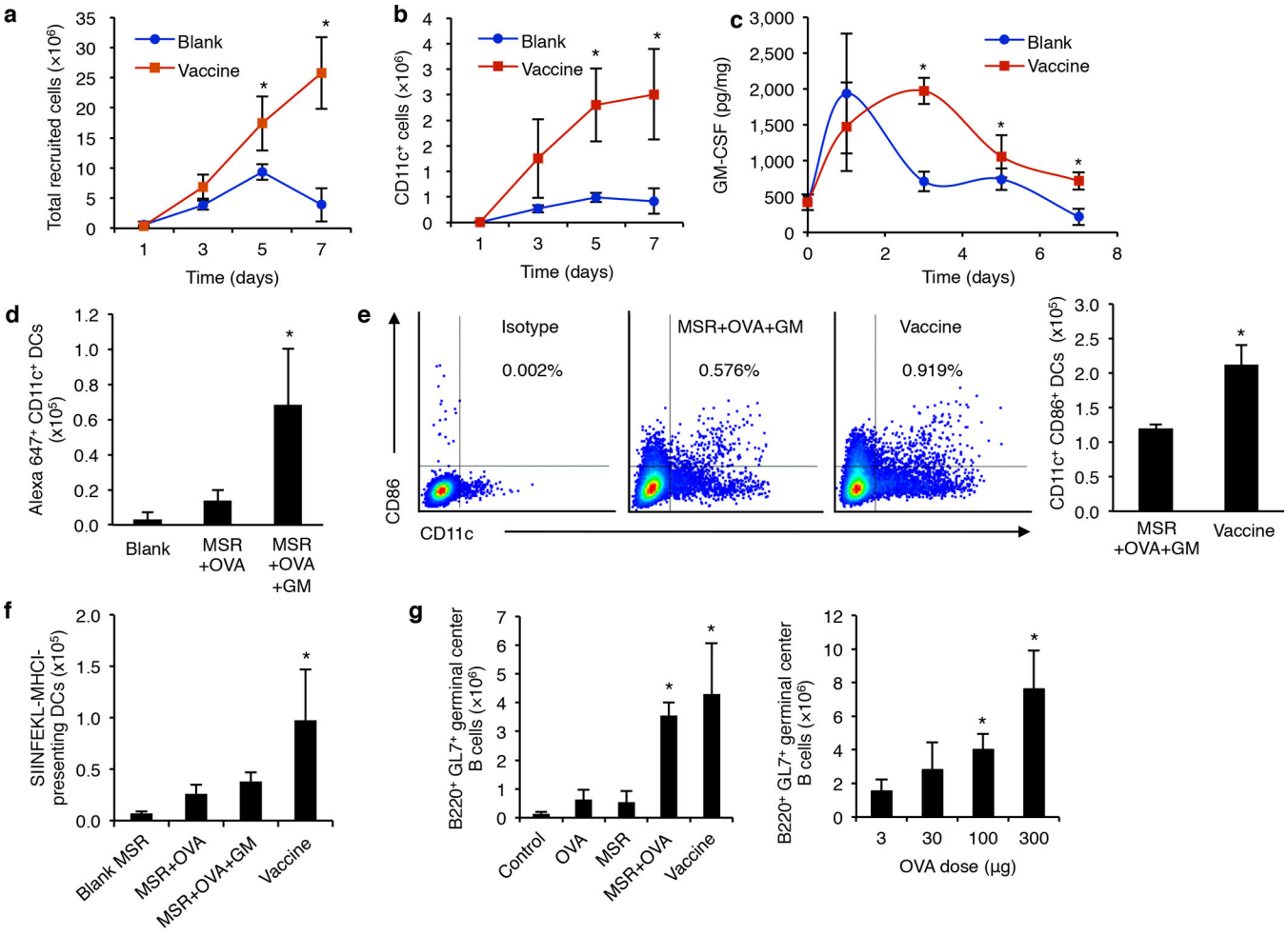

Figure 4. Vaccine formulation consisting of MSRs loaded with GM-CSF, CpG, and OVA is able to recruit DCs, program them with antigen and PAMP, and enhance their trafficking to the dLN to exert systemic effects

(a,b) Total number of recruited host cells (a) and $CD11c^+$ DCs (b) in blank or vaccine MSR scaffolds (5 mg), respectively (n=4). **(c)** *In vivo* GM-CSF levels in tissue around the injection sites of blank or vaccine MSR scaffolds (n=4). In (a–c), the comparisons were made between two groups (vaccine versus blank). **(d)** Numbers of Alexafluor 647^+ DCs in dLNs after injections of blank MSR scaffold, MSRs loaded with OVA*, or MSRs loaded with OVA* and GM-CSF, respectively (n=4). **(e)** Representative flow cytometry plots to analyze activated $CD11c^+$ $CD86^+$ DCs in dLNs in mice immunized with MSRs loaded with OVA/GM-CSF or MSRs loaded with OVA/GM-CSF/CpG (Vaccine), respectively (left), and numbers of $CD11c^+$ $CD86^+$ DCs in dLNs (right) (n=4). **(f)** Numbers of DCs presenting SIINKEKL-MHCI in dLNs at day 7 post immunization (n=4). **(g)** Numbers of $B220^+$ $GL7^+$ germinal center B cells at day 7 post immunization in untreated mice or mice treated with MSR containing various cargoes (left), and impact of OVA dose on number of germinal center B cells (right) (n=4). Biological replicates were used and studies were repeated at least 2 times in the lab. Values represent mean and s.d. *represents $p<0.05$.

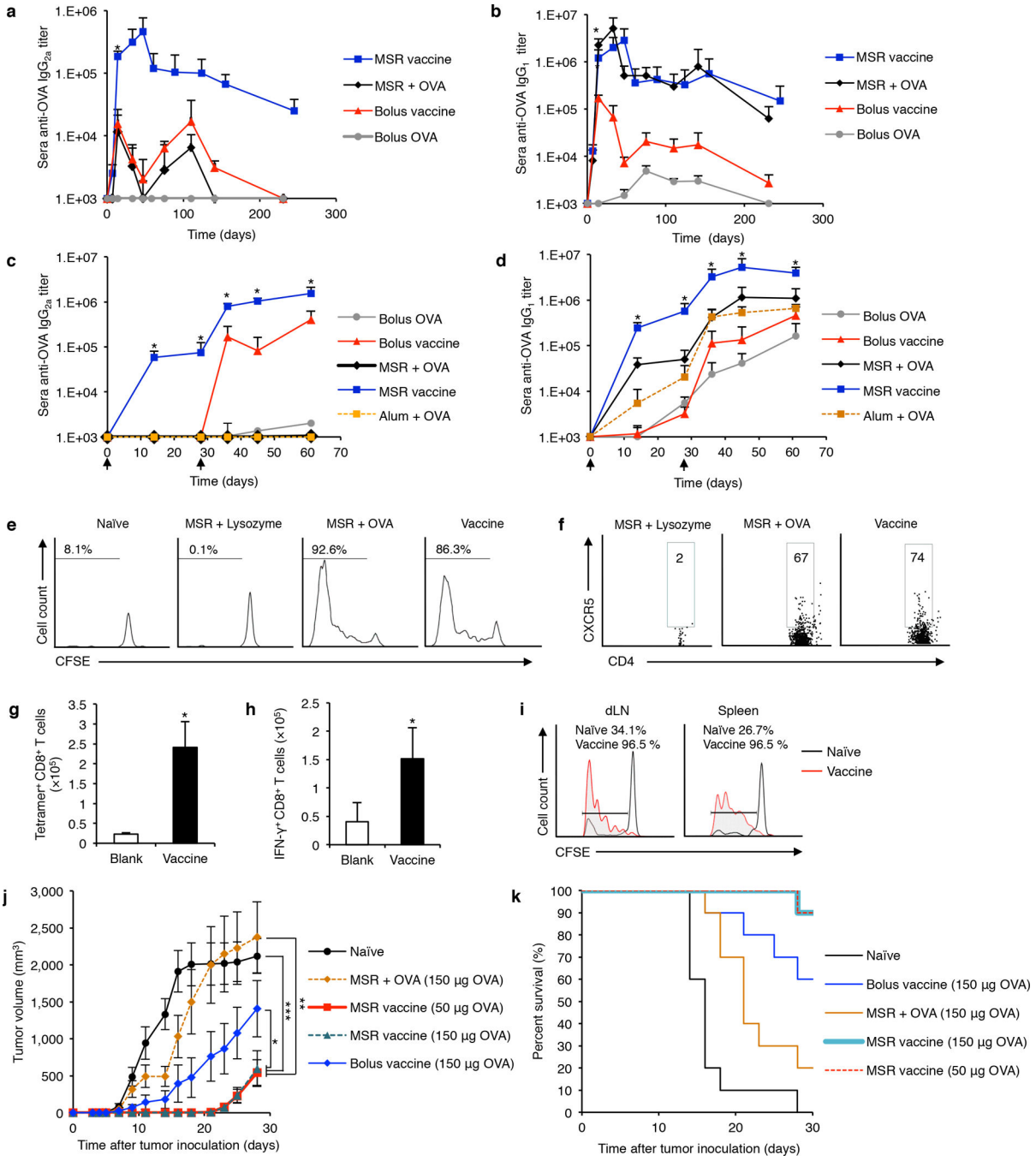

Figure 5. MSR vaccine generates potent humoral and cellular immune responses against a model antigen, OVA

(a,b) ELISA analysis of sera OVA-specific IgG_{2a} (a) or IgG_1 (b) after immunization with bolus OVA, soluble components of the vaccine (bolus vaccine), MSRs loaded with OVA, or MSR vaccine, respectively (n=5). **(c,d)** ELISA analysis of sera OVA-specific (c) IgG_{2a} and (d) IgG_1 after immunization with bolus OVA, bolus vaccine formulation (GM-CSF, CpG, OVA), Imject Alum with OVA, MSR with OVA, and the MSR vaccine formulation on day 0, and boosted with the same formulations for each condition on day 30 (n=5). In (a–d),

comparisons were made between vaccine and bolus formulation groups. **(e,f)** Flow cytometric analysis of proliferation of OVA-specific $CD4^+$ T cells (gated on $Thy1.2^+$ $CD3^+$ T cells) (e) and $CD4^+$ $CXCR5^+$ T follicular helper (T_{FH}) cells (gated on $Thy1.2^+$ $CD3^+$ T cells) (f) in naïve mice, or mice at day 3 post immunization with MSR loaded with non-specific antigen (MSR + Lysozyme), MSR loaded with OVA (MSR + OVA), or complete MSR vaccine (Vaccine) (n=4). **(g,h)** Number of $tetramer^+$ $CD8^+$ T cells (g) and IFN-γ^+ $CD8^+$ T cells (h) in spleen 7 days after vaccination with blank MSR (Blank) or complete MSR vaccine (Vaccine) (n=4). **(i)** Flow cytometric analysis of proliferation of OVA-specific $CD8^+$ T cells in the draining lymph node (dLN; left) and spleen (right) of naïve mice, and mice at day 3 post immunization with complete MSR vaccine (Vaccine). **(j,k)** Prophylactic cancer vaccine study using injectable MSRs. (j) EG.7-OVA tumor volume and (k) survival rate after subcutaneous injection of various vaccine formulations 10 days before tumor inoculation (n=10). In (j), the tumor volumes were compared on day 21, 23 and 25, following the onset of tumor growth in the vaccine group. Biological replicates were used and studies were repeated at least 2 times in the lab. Values represent mean and S.D. with exception of Fig. 5j, which is expressed as mean ± SEM. *, **, and *** represents $p<0.05$, $p<0.01$, and $p<0.001$, respectively.